Interior Pycnocline Flow from the Subtropical to the Equatorial Pacific Ocean*

GREGORY C. JOHNSON AND MICHAEL J. MCPHADEN

NOAA/Pacific Marine Environmental Laboratory, Seattle, Washington

(Manuscript received 5 May 1999, in final form 2 February 1999)

ABSTRACT

Interior circulation pathways from the subtropics to the equator are markedly different in the Northern and Southern Hemispheres of the Pacific Ocean. In the North Pacific the pycnocline shoals and strengthens dramatically under the intertropical convergence zone, separating the North Equatorial Current from the North Equatorial Countercurrent. While the high potential vorticity between these currents would intuitively seem to inhibit meridional water-property exchange between the subtopics and the equator, transient tracer analyses and some modeling studies have suggested an interior pathway from the subtropics to the equator in the pycnocline of the central North Pacific. This study delineates this pathway and estimates an upper bound for its magnitude at 5 ($\pm$1) $\times$ 10^9 kg s^{-1}. In contrast, the southern branch of the South Equatorial Current clearly brings pycnocline water estimated at 15 ($\pm$1) $\times$ 10^9 kg s^{-1} from the southern subtropics directly to the equator in the South Pacific through an interior region of low and relatively uniform potential vorticity. In both hemispheres, these interior pathways extend downward as far as the lightest waters of the equatorial pycnostad. The subsurface countercurrents flanking the pycnostad form the equatorward limbs of tropical subsurface cyclonic gyres. These deep gyres are consistent with the absence of interior ventilation of the equator from the subtropics below the pycnocline. Measured and derived fields from a hydrographic climatology are presented on neutral surfaces and in meridional–vertical sections to show that salinity, potential vorticity, and acceleration potential are all consonant with these arguments. The vertical extent of interior communication is also in agreement with the transient tracer results.

1. Introduction

Recently, it has been suggested (Gu and Philander 1997), supported by observational analysis (Zhang et al. 1998), that interior thermal anomalies, apparently originating where water is subducted in the subtropics of the North Pacific (Deser et al. 1996), may propagate to the equatorial region in the Pacific. This propagation may occur through advection by the ocean general circulation (Gu and Philander 1997), or more rapidly through Rossby and Kelvin waves (Lysne et al. 1997). Thermal anomalies may be owing to subduction poleward of 18°N and variations of wind stress equatorward of this latitude (Schneider et al. 1999). It has been further hypothesized that these anomalies may contribute to the decadal changes observed in the structure of the equatorial pycnocline and that this modulation of the equatorial pycnocline may in turn be linked to a shift in the dynamics, frequency, and intensity of El Niño (Gu and Philander 1997). Taken together, these hypotheses are one reason that the pathways by which and rates at which subtropical water reaches the equatorial region is of interest in understanding and predicting seasonal-to-interannual climate variability. Of course, describing intergyre oceanic mass and water property exchanges, understanding their dynamics, and quantifying their magnitudes are also important in themselves to the study of the ocean general circulation and its role in climate.

Tritium data have been interpreted to suggest an interior pathway along which pycnocline water ventilated in the subtropical North Pacific reaches the equator between 145°W and 125°W (Fine et al. 1987) in the central Pacific, crossing the intertropical convergence zone (ITCZ) that separates the westward North Equatorial Current (NEC) from the eastward North Equatorial Countercurrent (NECC). These data suggest this northern ventilation ranges in potential density from σ_θ = 23 to 26.2 kg m^{-3} and that at σ_θ = 25.0 kg m^{-3} the timescale for water to reach the equator is less than 14 years.

Depth-integrated geostrophic mass transport in the North Pacific Ocean as inferred from Sverdrup dynamics clearly indicates this interior pathway (McPhaden and Fine 1988). In addition, mean surface dynamic height relative to a pressure of 1000 dbar (Wyrtki 1975)

* PMEL Contribution Number 1966.

Corresponding author address: Dr. Gregory C. Johnson, NOAA/Pacific Marine Environmental Laboratory, 7600 Sand Point Way N.E., Bldg. 3, Seattle, WA 98115-0070.
E-mail: gjohnson@pmel.noaa.gov

shows a similar pattern. However, water in the ocean interior moves along neutral surfaces. The near-surface geostrophic circulation likely has a pattern similar to the surface dynamic height field or the depth-integrated mass transport predicted using the wind stress curl, but these studies do not reveal how the circulation changes with increasing density (and depth).

Modeling provides a third approach to the question of pathways for subtropical–equatorial exchange. Ventilated thermocline dynamics (Luyten et al. 1983), extended to the Tropics in a reduced-gravity model formulation, shows that the presence of an interior pathway for Northern Hemisphere ventilation depends critically on the location of the poleward edge of the shadow zone (McCreary and Lu 1994; Liu 1994). A complex configuration of the model with a Pacific-like geometry under a smoothed climatological wind field suggests that the region of high potential vorticity beneath the ITCZ may constitute a barrier to interior subtropical–equatorial exchange in the Northern Hemisphere (Lu and McCreary 1995). However, reducing the model thermocline thickness to a smaller value results in an interior pathway as one of three possibilities (Lu et al. 1998; Liu and Huang 1998).

Lagrangian analysis of more complex ocean general circulation models also shows that water subducted in the Northern Hemisphere subtropics takes one of three pathways (Liu et al. 1994; Gu and Philander 1997; Liu and Huang 1998; Rothstein et al. 1998). Water subducted in the western North Pacific reaches the western boundary and heads north in the Kuroshio, avoiding immediate subtropical–equatorial exchange. Water subducted in the central North Pacific reaches the western boundary and heads south in the Mindanao Current to join the eastward flowing Equatorial Undercurrent (EUC), after reaching the date line in the NECC. Water subducted in the eastern North Pacific describes a zigzag toward the equator, initially flowing southwestward in the NEC, then abruptly turning south to flow southeastward in the NECC, then turning south again to flow southwestward in the northern branch of the South Equatorial Current (SEC) before joining the EUC in the central Pacific. In the Southern Hemisphere subtropics the three pathways for subducted water are similar, with the significant exception that the waters subducted farthest east flow directly northwestward toward the equator in the southern branch of the SEC. In general, water parcels take under 16 years to reach the equatorial region after subduction (Gu and Philander 1997), roughly consonant with the time estimated from the tritium measurements (Fine et al. 1987).

A comprehensive description of the tropical Pacific Ocean circulation and its variation with density using conventional physical oceanographic measurements exists (Tsuchiya 1968). The work here adds to this description with discussions of potential vorticity, vertical sections, and an emphasis on interior pathways for subtropical–equatorial exchange, only briefly discussed in Tsuchiya (1968). In addition, 25 times more stations are used than were available to Tsuchiya (1968), and the present data are all high vertical resolution CTD data rather than the bottle data used before. Maps of depth, salinity, potential vorticity, and acceleration potential on selected neutral surfaces are discussed along with meridional–vertical sections of neutral density, salinity, and potential vorticity. The density above which interior subtropical-to-equatorial exchange ceases in both hemispheres is quantified and shown to coincide with the base of the tropical pycnocline. This density surface outcrops in winter at the poleward limits of the subtropical gyres. It is also the density above which the equatorial pycnostad and the eastward flowing Tsuchiya jets, that is, the North and South Subsurface Countercurrents (NSCC and SSCC, or SCCs), are found (Tsuchiya 1975; Johnson and Moore 1997; Rowe et al. 2000). These jets form the equatorward limbs of basin-wide subsurface cyclonic tropical gyres, where equatorward flow is absent except at the western boundary. Finally, interior meridional transport estimates within the tropical pycnocline are presented.

2. CTD data processing

For this study, CTD stations within areal bins in the tropical Pacific are averaged to make a mean hydrographic profile for each bin. In latitude, the bins are centered every 1° from 20°S to 20°N. In longitude, the bins are centered every 5° from 120°E to 75°W. This anisotropy is dictated by the data distribution, consisting mostly of closely sampled meridional sections with wide zonal spacing, but is also appropriate to the tropical ocean interior where zonal scales greatly exceed meridional scales. For this study 15 693 individual CTD stations between 20.5°S and 20.5°N, 120°E and 70°W and taken from 1967 through 1998 are used. These data are all the high-resolution profiles available from the National Oceanographic Data Center (NODC) archives, as well as recent Pacific Marine Environmental Laboratory (PMEL) cruise data and some other cruise data not yet available from NODC. The average profiles are used to make maps of properties on neutral density anomaly, γ_n, surfaces (Jackett and McDougall 1997), meridional–vertical water property sections, and mass transport estimates. Only profiles with more than two CTD casts are used for the property maps and transport estimates and with two or more CTD casts for the vertical sections.

The CTD station data within each bin, consisting of salinity S and temperature T as a function of pressure P are averaged as a function of γ_n to create mean hydrographic profiles. Averaging S, T, and P as functions of γ_n is more involved than the conventional approach of averaging S, T, and γ_n as functions of P, but this technique better preserves water properties in the sharp tropical pycnocline and the strength of the pycnocline itself because averaging is quasi-Lagrangian in the vertical (Gouriou and Toole 1993). First, to reduce small-

scale noise, individual CTD station S and T profiles are filtered in P with a 5-dbar half-width Hanning filter and subsampled at 5-dbar intervals. Then γ_n is computed for these subsampled data and averaged as a function of P to obtain a mean $\gamma_n(P)$ profile at 5-dbar resolution. Following this step, the individually filtered and sampled profiles of S, T, and P are linearly interpolated to each $\gamma_n(P)$ profile value to allow averaging of the individual CTD station data as a function of γ_n at roughly 5-dbar resolution. Mean profiles for $S(\gamma_n)$, $T(\gamma_n)$, and $P(\gamma_n)$ are then calculated. Finally the mean $P(\gamma_n)$ profile is used to put the mean profiles of $S(\gamma_n)$ and $T(\gamma_n)$ onto an even 5-dbar grid and construct a final mean γ_n profile. The profile is limited to values denser than the densest mixed layer for the CTD stations within the bin.

Depth and properties of the surface mixed layer, including γ_n, vary over time. To construct a mixed layer for the mean profiles of $S(\gamma_n)$, $T(\gamma_n)$, and γ_n, the following procedure is used. First, the mixed layer P for each CTD station is defined as the P above which γ_n is less than 0.05 kg m^{-3} denser than the mean γ_n of the top 10 dbar. Mean S and T from the surface to the mixed layer P are calculated for each CTD station. Then these S and T values are averaged to find mean mixed layer values for S and T. These values are used with the mean mixed layer P to calculate a mean mixed layer γ_n. In order to avoid γ_n inversions in the mean profiles, the pressure of the mean mixed layer γ_n in the final mean γ_n profile is used to define a final mean mixed layer P. To finish, the mean mixed layer S, T, and γ_n values are substituted into the mean $S(\gamma_n)$, $T(\gamma_n)$, and γ_n profiles from the mean mixed layer P to the surface. The gap between the mean mixed layer and the mean interior profiles is interpolated using a shape-preserving local spline (Akima 1970).

The analysis exclusively uses the resulting 5-dbar mean hydrographic profiles. The only further vertical smoothing performed is on the square of the buoyancy frequency, N^2, which is calculated from the mean hydrographic profiles and then smoothed with a 35-dbar median filter before use. The median filter effectively reduces noise while preserving the rapid transition from the surface mixed layer to the pycnocline. This quantity is then used to calculate the planetary component of the potential vorticity, $Q = N^2 f/g$. A few Q profiles still have some noise at depth in bins with few stations and some of those ending in shallow water. Neutral surface maps are made by linearly interpolating the 5-dbar values of each mean hydrographic profile to the appropriate γ_n. These values are then objectively mapped assuming a Gaussian covariance with correlation length scales of 10° longitude and 2° latitude and a noise-to-signal variance ratio of 0.25. These correlation length scales are twice the bin size, to emphasize only those large-scale features that are well resolved by the data.

3. Water property maps on neutral surfaces

Here properties on two neutral surfaces are discussed. The lighter surface, $\gamma_n = 25.0$ kg m^{-3}, is chosen for proximity to the equatorial pycnocline, the EUC, and the subtropical mode water (STMW) vertical potential vorticity minima (best seen in the meridional–vertical sections discussed below). The denser surface, $\gamma_n = 26.5$ kg m^{-3}, is chosen to lie below the pycnocline, but within the equatorial pycnostad and the SCCs. Winter outcropping locations of the lighter surface are in the subtropics and the denser surface in the subpolar regions (Fig. 1). Depth locates the neutral surface and its gradients give a sense of vertical geostrophic shear. Acceleration potential contours are streamlines of geostrophic velocity on that surface relative to 900 dbar. Salinity on a neutral surface is a passive tracer inversely related to temperature since saltier water must be cooler and fresher water must be warmer to remain on the neutral surface. Finally, the planetary component of the potential vorticity is a dynamically active tracer that (away from the equator and the western boundary) has seldom been described in the Tropics, but see Gouriou and Toole (1993). In the absence of mixing and boundary forcing, both salinity and potential vorticity are conservative on neutral surfaces. However, in the ocean, these properties are not strictly conserved. Their distribution on neutral surfaces is governed by both advection and diffusion.

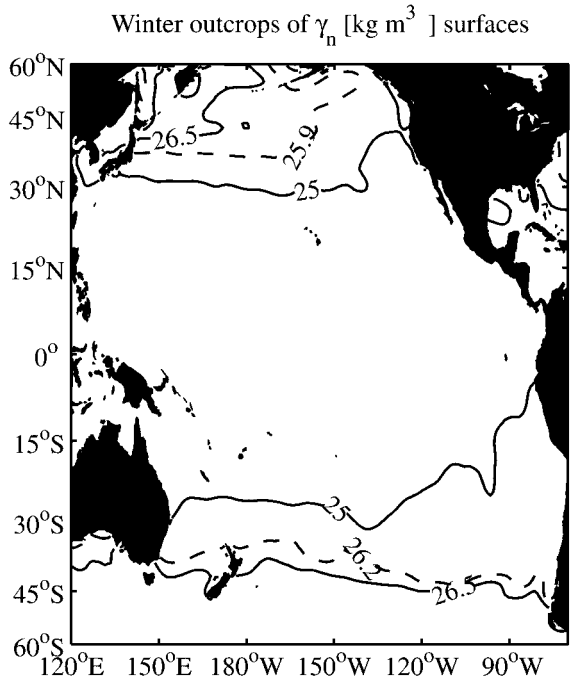

FIG. 1. Winter (Jan–Mar in the north and Jul–Sep in the south) surface outcrops of $\gamma_n = 25.0$ and 26.5 kg m^{-3} and the pycnocline base (dashed lines) from seasonal climatologies of temperature (Levitus and Boyer 1994) and salinity (Levitus et al. 1994).

The $\gamma_n = 25.0$ kg m^{-3} surface has a specific volume anomaly of 301($\pm$2) $\times$ 10^{-8} m^3 kg^{-1} and a potential density anomaly of 24.984($\pm$0.004) kg m^{-3}, very close to the second lightest surface of Tsuchiya (1968). The

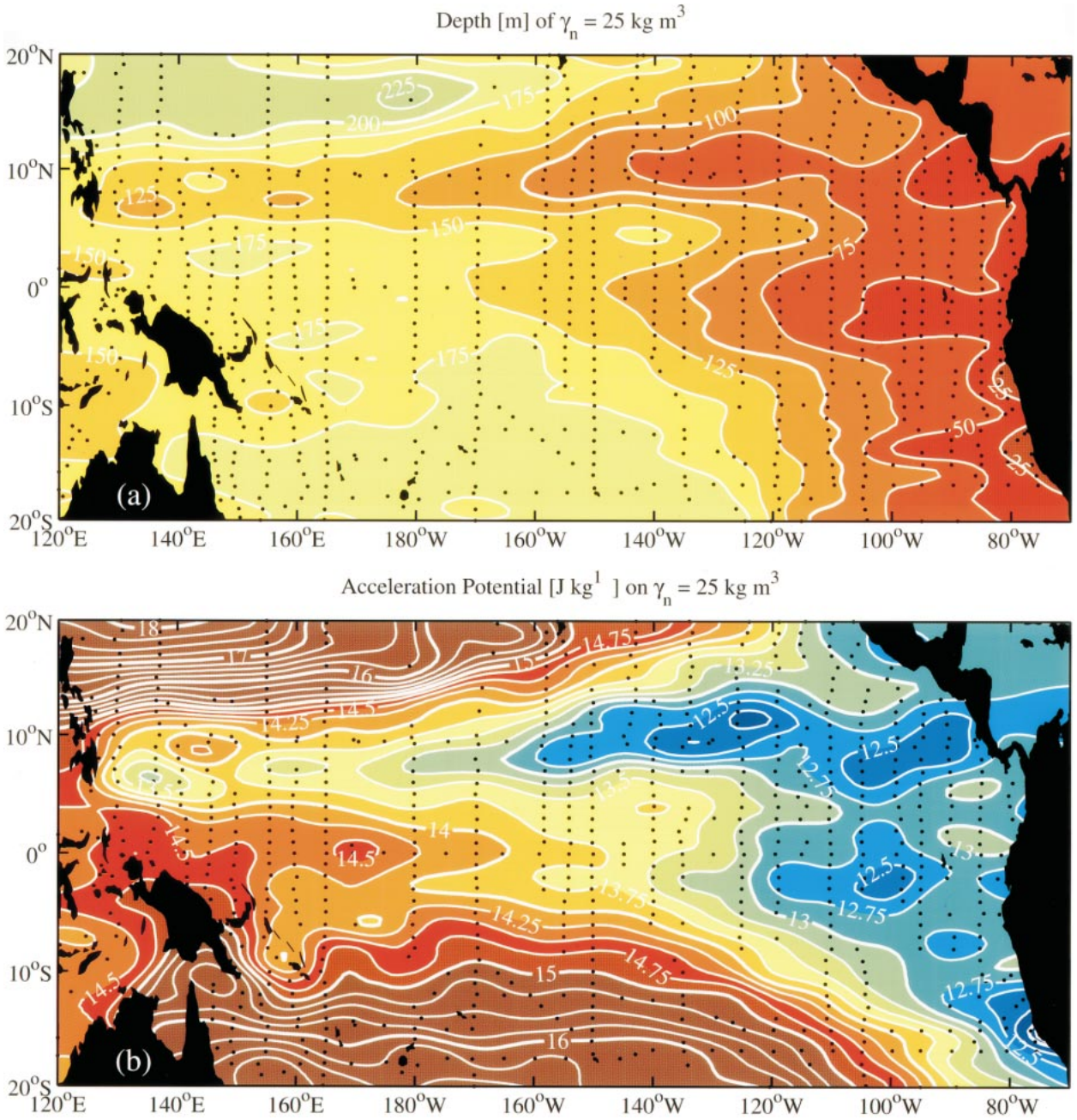

FIG. 2. Maps of properties on γ_n = 25.0 kg m^{-3}, within the tropical pycnocline. Color palettes are consistent for Figs. 2–5 except for acceleration potential, which has a varying offset. The locations of the mean hydrographic profiles (black dots) are given by the average positions of the CTD stations within bins mentioned in section 2. All panels are objectively mapped from values at these locations. (a) Depth contour intervals of 25 m. (b) Acceleration potential relative to 900 dbar; contour intervals of 0.25 J kg^{-1}.

Northern and Southern Hemisphere patterns differ largely. Depth (Fig. 2a) shoals from over 225 m in the northwest part of the region to less than 25 m off South America. A nearly zonal ridge starts at 7°N off the western boundary, reaches 11°N by 125°W, and terminates at its shallowest in the Costa Rica Dome (somewhat obscured in this large-scale climatology) at 9°N, 90°W (Hoffman et al. 1981). This ridge lies below the upwelling-favorable wind stress associated with the ITCZ and separates the NEC and the NECC. A nearly zonal trough starts at 3°N off the western boundary and reaches 5°N by 105°W. East of 150°W, this trough separates the NECC to the north from the SEC to the south. A ridge along the equator marks the dome associated with the upper part of the EUC and separates the northern and southern branches of the SEC. At the southern edge

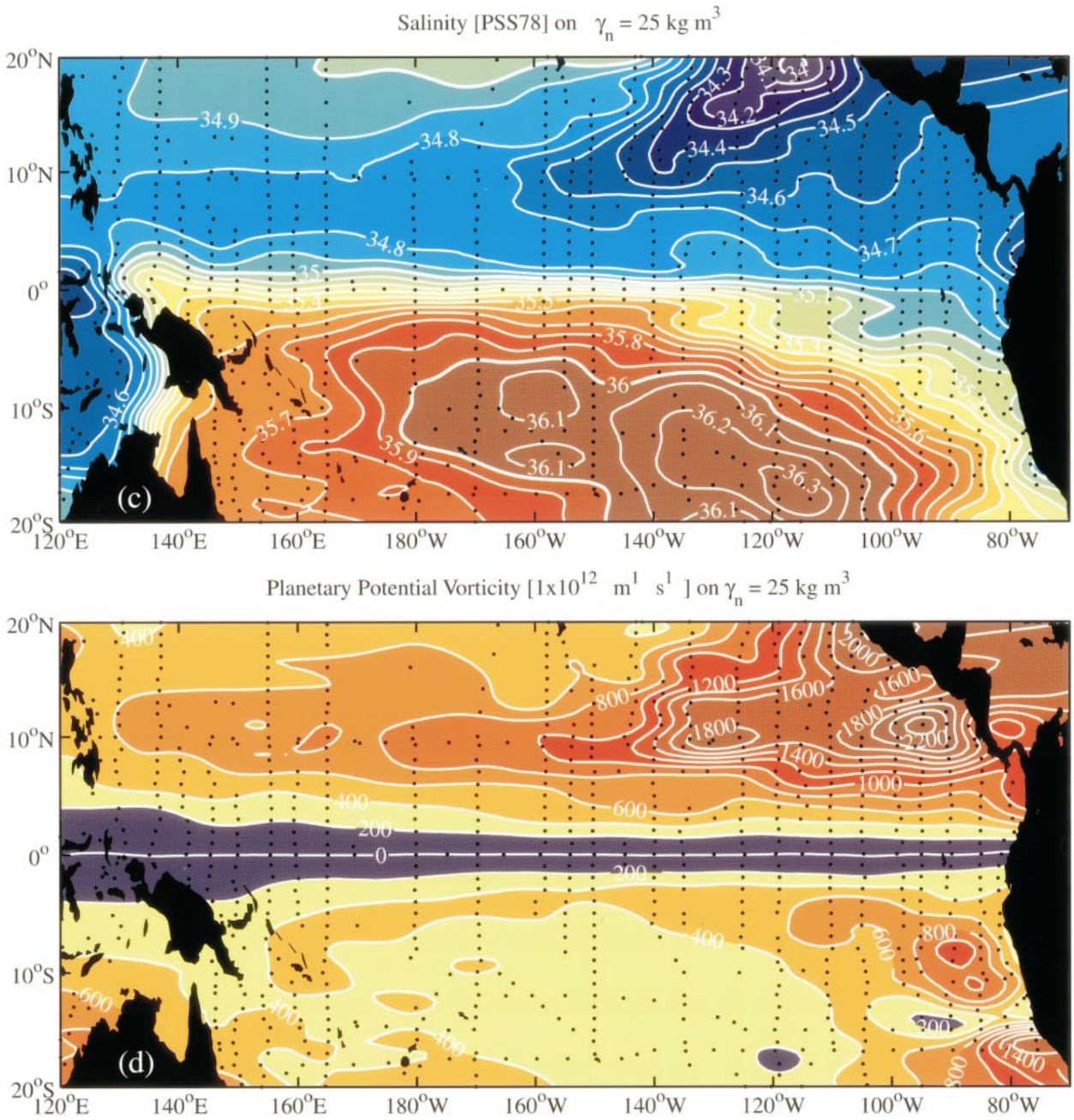

FIG. 2. (*Continued*) (c) Salinity, contour intervals of 0.1 (PSS-78). (d) Planetary potential vorticity, contour intervals of 200×10^{-12} m^{-1} s^{-1}.

a marked eastward shoaling occurs about 120°W, with isobaths fanning out equatorward and westward, a signature of the SEC. At least some of the shoaling just off South America is owing to upwelling-favorable alongshore winds there.

Acceleration potential on this surface (Fig. 2b) has a similar pattern to that of depth, but reversed in sign. A trough extends from 6°N off the western boundary to 11°N, 125°W and terminates around 9°N, 90°W. The eastward fall of values along this trough from 165°E to 135°W reveals interior flow southward from the NEC into the NECC. Most of these isopleths can be traced northeast, originating off North America. While the eastern part of this southward flow may be part of a tropical recirculation centered at 11°N, 125°W, this pattern is weaker on lighter neutral surfaces (not shown). A ridge on the equator with values falling between the date line and 105°W suggests equatorward pycnocline convergence feeding the EUC. In the north, between the date line and 150°W the NECC supplies this conver-

gence from the western boundary. From 150° to 100°W a ridge at 3°–4°N separates the NECC from the SEC. Values falling eastward along this ridge again indicate some southward interior flow from the NECC into the SEC and subsequent convergence on the equator to feed the EUC. These southward flows from the NEC to NECC starting at 165°E extending at most to 135°W and from the NECC to the SEC from 150° to 100°W allow a somewhat convoluted interior route for subtropical water from the northeast Pacific to reach the EUC.

The Southern Hemisphere is simpler, lacking an ITCZ except in the west. Values of acceleration potential (Fig. 2b) generally fall equatorward and eastward to a trough at 3°–2°S from the date line to about 100°W. This trough separates the SEC from the EUC. The falling values all along this trough suggest a direct interior route for subtropical water to reach the EUC from the southeast Pacific. However, west of the date line a trough is evident at 6°S in the vicinity of the South Pacific convergence zone, blocking the interior route to the equator. Eastward flow north of this trough may be related to the South Equatorial Countercurrent (SECC). However, this surface is too dense to fully reveal the SECC. In the west the SEC feeds the New Guinea Coastal Undercurrent (Tsuchiya et al. 1989).

Salinity on this surface (Fig. 2c) is relatively high in the north-central Pacific, owing to a shallow salinity maximum of the North Pacific tropical water (NPTW; Tsuchiya et al. 1989) at $\gamma_n = 24.3$ kg m^{-3}. The NPTW is swept westward and slightly southward in the NEC. The southeast Pacific is very salty, owing to the strong South Pacific tropical water (SPTW) salinity maximum at $\gamma_n = 24.6$ kg m^{-3}. The SPTW is swept westward and equatorward in the SEC. In the northeast Pacific, fresher California Current water (CCW; Tsuchiya 1968), with a salinity minimum at $\gamma_n = 24.8$ kg m^{-3}, sweeps southward and westward in the NEC, forming the relative minimum on this surface that separates the NPTW and SPTW. In addition, the denser salinity minimum at $\gamma_n = 26.7$ kg m^{-3}, a signature of the North Pacific Intermediate Water (NPIW), may exert some influence, even at this shallow surface, through diapycnal fluxes into the strong shallow pycnocline under the ITCZ. Finally, freshness from excess rainfall under the ITCZ may also mix down to this surface. The equatorial convergence (Fig. 2b) of these three fresh northern sources and the salty SPTW creates a strong meridional salinity gradient at the equator. Slight northward penetration of SPTW across the equator is evident near the western boundary. In addition, the meridional salinity maximum at 1°S between 135° and 100°W is owing to SPTW advected eastward in the EUC.

The planetary component of potential vorticity on this surface (Fig. 2d) also exhibits contrasting patterns in the Northern and Southern Hemispheres. At the northern edge low potential vorticity, especially from 160° to 125°W, is the remnant of eastern STMW (discussed below) formed to the north. Under the ITCZ values peak at 10°N, 125°W and again at 11°N, 95°W. This peak under the ITCZ is where the pycnocline is drawn closest to the surface by Ekman pumping associated with the large-scale wind stress curl and strengthened, perhaps by some combination of mixing and surface buoyancy flux. The pattern there is striking because acceleration potential contours (Fig. 2b) parallel isovorts (Fig. 2d), showing how the southward flow from the NEC to the NECC does not cross the high potential vorticity under the ITCZ, but moves around it. In the Southern Hemisphere, where the sign of potential vorticity is reversed, the only high magnitudes are off South America, where the pycnocline shoals and strengthens. Elsewhere, potential vorticity is low and relatively uniform. This pattern is associated with eastern STMW that has a vertical minimum around $\gamma_n = 25.3$ kg m^{-3}, visible in vertical sections. This minimum is strongest at the southern boundary around 120°W where the surface shoals rapidly from west to east (Fig. 2a). The uniformity of potential vorticity in the Southern Hemisphere shows that there is no impediment to direct interior convergence of water from the subtropics to the equator in the SEC. Finally, isovorts around the equator are spread in the west and pinched in the east, a pattern consistent with acceleration potential and salinity distributions that suggest equatorward interior pycnocline convergence feeding the EUC.

The $\gamma_n = 26.5$ kg m^{-3} surface has a specific volume anomaly of $165(\pm 2) \times 10^{-8}$ m^{-3} kg^{-1} and a potential density anomaly of $26.438(\pm 0.006)$ kg m^{-3}, close to the densest surface described by Tsuchiya (1968). The fields for this surface are markedly different from those within the pycnocline. Poleward and westward the depth of this surface (Fig. 3a) exceeds 500 m in the NEC and 425 m in the SEC. A ridge under the ITCZ starts at 6°N off the western boundary, peaks at less than 150 m at 10°N, 135°W, and extends eastward to 7°N, 100°W. In the Southern Hemisphere, a similar ridge starts at 3°S off the western boundary and turns at 150°W to reach 15°S off South America. It is shallowest near 9°S, 95°W. An equatorial trough, from bowing at the base of the EUC, deepens toward both boundaries.

Acceleration potential (Fig. 3b) again has some inverse correlation with depth. A nearly zonal trough starts at 5°N off the western boundary and reaches 6°N by 100°W. This trough delineates a cyclonic gyre with a narrow, rapid equatorward limb (the NSCC) and a wider, slower poleward limb starting at 20°N, 120°W and reaching 10°N by the western boundary (the deep NEC). These limbs are clearly connected by southward flow in the west and northward flow in the east. In the south, an analogous, but more tenuous gyre defined by the 11.5 J kg^{-1} contour starts at 5°S in the west and reaches 15°S just off South America. The SSCC forms the equatorward limb and the deep SEC the poleward limb. The poleward flow connecting these currents in the east probably occurs so close to the continent that it is not

resolved by the climatology, although diapycnal mixing may also play a role in the mass balance near the eastern boundary. Acceleration potential does not reveal flow at very low latitudes, but direct velocity measurements there suggest some westward return flow equatorward of the SCCs, implying deep anticyclonic gyres (Rowe et al. 2000). Notably, all these gyres effectively isolate the equator from deep interior subtropical ventilation.

This surface is fresh at the northern edge, owing to the combined influence of lighter CCW to the east and denser NPIW to the west (Fig. 3c). In the southeast the fresh influence of Antarctic Intermediate Water (AAIW), a vertical salinity minimum at $\gamma_n = 27.2$ kg m^{-3}, is evident. Higher Coral Sea and equatorial values encompassed by the 34.8 isohaline are owing to the mixing of salt from above. The meridional maximum starting at 4°S off the western boundary and reaching 7°S off South America is consistent with eastward advection in the SSCC. The salinity front at 2°N off the western boundary, reaching 4.5°N by 105°W (Fig. 3c), suggests that there is little meridional flow across the NSCC (Gouriou and Toole 1993). Similarly, another front starting at 10°N off the western boundary and reaching 20°N by 110°W suggests that meridional flow is also small at the northern limb of the deep gyre. The relatively homogenous region between these fronts, with slightly fresher subtropical waters advected eastward in the equatorward limb of the gyre and slightly saltier equatorial waters advected westward in the northern limb, is consistent with a tracer swirling around the gyre edge and homogenizing in the gyre interior.

Potential vorticity on this surface (Fig. 3d) increases nearly monotonically in magnitude poleward. However, lower values in the east are associated with the thickening equatorial pycnostad. In the Southern Hemisphere, a strong meridional front separating the equatorial pycnostad from the subtropical waters is evident, starting at 3°S off the western boundary and reaching 15°S off South America. This front runs along the SSCC, suggesting an absence of meridional exchange across this current. In the Northern Hemisphere, a similar front starts at 2°N off the western boundary and extends to about 5°N, 105°W. As in the salinity field, there is another front associated with the northern limb of this deep cyclonic gyre starting at 20°N, 110°W and reaching 10°N off the western boundary. Also paralleling the salinity field, between these fronts there is a relatively homogenous region where high subtropical values are advected eastward in the NSCC and low tropical values are swept northward in the eastern Pacific and then westward in the deep NEC. The low values under the ITCZ and off the South American coast suggest that upwelling-driven vortex stretching below the pycnocline is associated with the poleward transport in the deep cyclonic gyres.

In summary, property maps on two neutral surfaces highlight differences between the two hemispheres within the tropical pycnocline as well as changes at the pycnocline base. The pycnocline shoals from west to east, and under the ITCZ. In the north, equatorward flow of relatively fresh pycnocline water follows a serpentine route to skirt westward of the eastern potential vorticity maximum under the ITCZ. In the south, relatively salty pycnocline water follows a much more direct interior route to the equator through a region of homogenous and low potential vorticity characteristic of strong eastern STMW there. Below the pycnocline, deep cyclonic gyres are evident in each hemisphere, precluding any interior equatorward flow there. Acceleration potential, salinity, and potential vorticity distributions are consistent with advection around these deep gyres, and homogenization within them, especially in the Northern Hemisphere.

4. Meridional–vertical water property sections

To complement the maps on neutral surfaces, two sets of meridional–vertical sections are compared and contrasted, one along 165°E, representative of the western Pacific, and another along 125°W, representative of the eastern Pacific. These sections are similar in areal extent to a set of mean sections used to discuss currents and water masses in the central Pacific (Wyrtki and Kilonsky 1984). Sections of salinity and planetary potential vorticity are displayed with neutral surfaces (referred to as isopycnals) overlaid and are discussed as tracers of the net meridional circulation and the deep cyclonic gyres.

The latitude ranges, maximum densities and pressures, and core densities and pressures of the quasi-zonal tropical currents (Table 1) generally shoal with the pycnocline, tilted upward to the east by the trade winds, and shift poleward from west to east. The eastward-flowing Subtropical Countercurrent (STCC), associated with northward isopycnal spreading in the STMW, is only present at 165°E where the STMW is strong. The NEC at 125°W is poleward of its location at 165°E where its northern end flows beneath the STCC. The NECC at 125°W is also poleward and shallower than it is at 165°E. The maximum extents and cores of the SCCs are poleward, shallower, and lighter at 125°W than at 165°E. Unlike at 165°E, these currents are easily distinguished from the EUC and the NECC at 125°W. The EUC is shallower and lighter at 125°W than at 165°E. The north branch of the SEC at 125°W is shallower, lighter, and extends farther north than at 165°E. The south branch of the SEC at 125°W is shallower, lighter, and stronger than at 165°E. The SECC is only evident at 165°E. These zonal shifts imply geostrophic equatorward convergence within the pycnocline and divergence below it.

At 165°E (Fig. 4a), the NPTW salinity maximum at $\gamma_n = 24.0$ kg m^{-3} near 20°N is reduced, partly owing to zonal flow, under the ITCZ around 8°N between the fresh surface waters and the NPIW. Here the NPIW salinity minimum near $\gamma_n = 26.8$ kg m^{-3} at 20°N dominates the fresh northern water approaching the equator

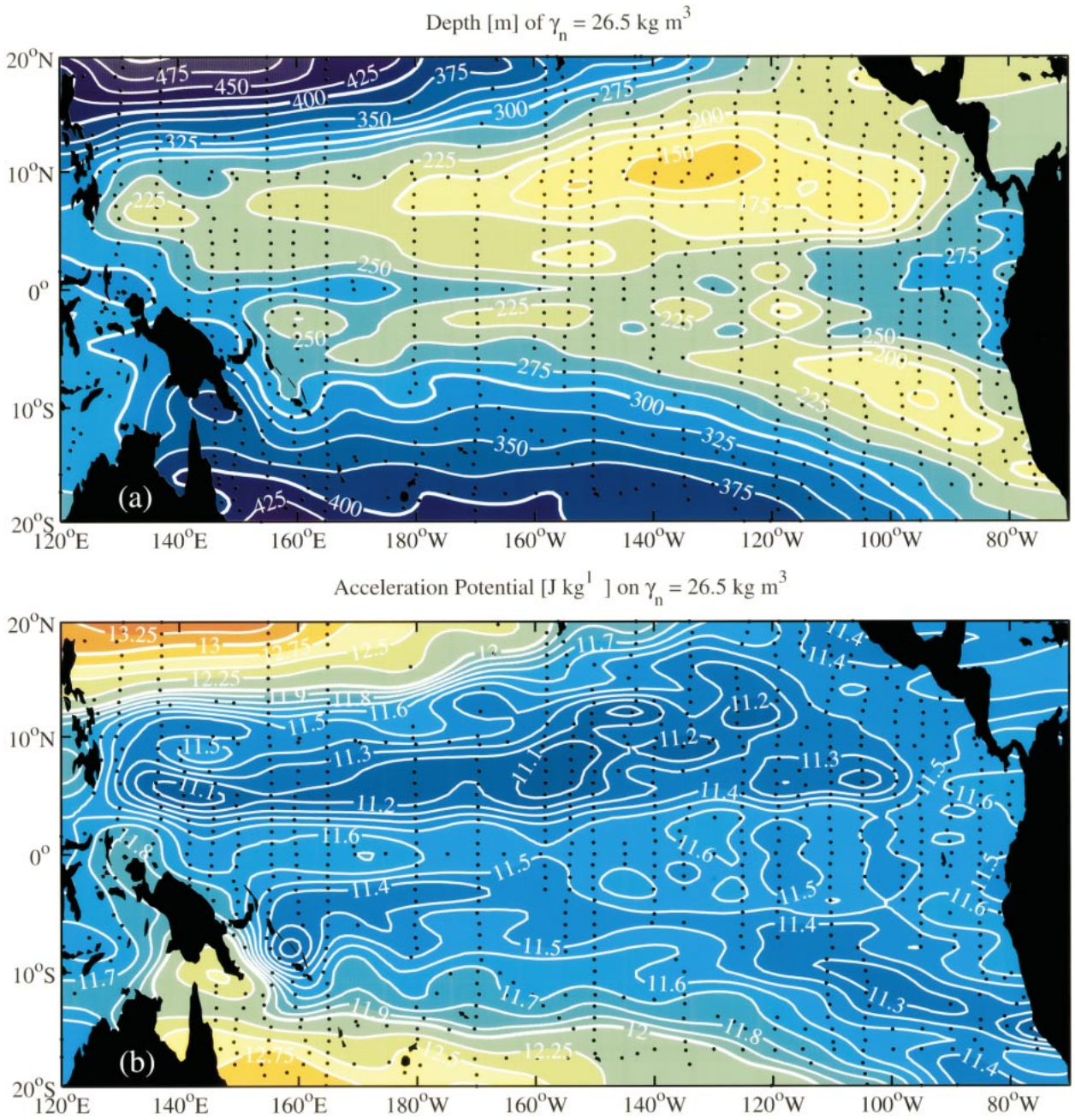

FIG. 3. Maps of properties on γ_n = 26.5 kg m^{-3}, below the tropical pycnocline. Details follow Fig. 2. (a) Depth, contour intervals of 25 m. (b) Acceleration potential relative to 900 dbar, contour intervals varying from 0.1 to 0.25 J kg^{-1}.

along serpentine routes, lightening to γ_n = 26.1 kg m^{-3} by 1°N. This density shift of the salinity minimum is realized because only the lightest portion of the NPIW influence flows toward the equator in the interior and that from the western boundary flows east in the NSCC. In the south, fresh AAIW is noticeable at depth. The SPTW salinity maximum contrasts strongly with the fresh northern water, as both converge on the EUC. The interruption of the 35.8 isohaline at 10°S is associated with fresh eastward flow in the SECC. Around γ_n = 26.8 kg m^{-3} a southern salty influence can be seen within the entire deep equatorial pycnostad between 3°S and 3°N. The local meridional minimum at 5°N, the northern edge of the NSCC, is advected eastward, as are slightly salty waters at 5°S in the southern edge of the SSCC. Around this same density, a homogenous local vertical maximum between 5° to 11°N and 250 to 450 m is the result of mixing at the center of the deep cyclonic gyre. This gyre separates the fresh waters to the north from the saltier equatorial waters.

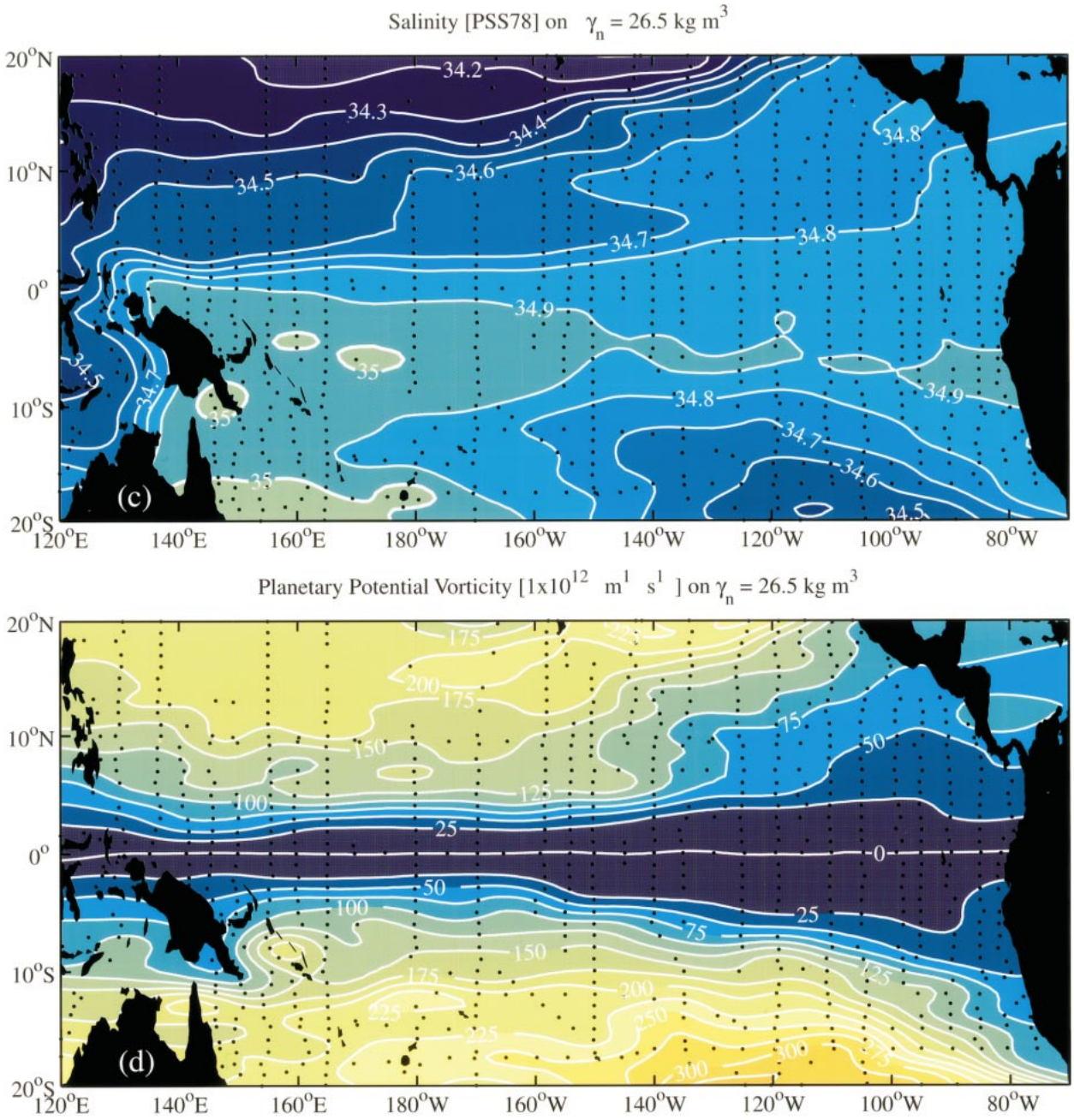

FIG. 3. (*Continued*) (c) Salinity, contour intervals of 0.1 (PSS-78). (d) Planetary potential vorticity, contour intervals of 25 × 10^{-12} m^{-1} s^{-1}.

At 125°W (Fig. 4b) the salinity minimum is shallower and lighter than at 165°E; CCW influence at γ_n = 25.5 kg m^{-3} near 20°N persists as a subtle vertical minimum to 1°N at γ_n = 25.0 kg m^{-3}, roughly following neutral surfaces on its serpentine equatorward path. Where the pycnocline is shallowest, around 12°N, the fresh surface influence of precipitation under the ITCZ may augment that of the CCW. The northern deep salinity minimum is much weaker and denser than at 165°E, reflecting an absence of NPIW influence here. The AAIW salinity minimum around γ_n = 27.2 kg m^{-3} at 20°S is stronger than at 165°E, being closer to the southeast Pacific where AAIW is freshest. Above the AAIW is the strong SPTW salinity maximum at γ_n = 24.5 kg m^{-3}. This maximum is formed by excess evaporation over precipitation where the neutral surface outcrops in the southeast Pacific, which is why it is stronger here than at 165°E. An isolated vertical maximum at 1°S, γ_n = 25.0 kg m^{-3} (not visible in Fig. 4b, but see Fig. 2c) is SPTW advected eastward in the EUC, where convergence creates a strong contrast with fresher northern water. Around γ_n = 26.5 kg m^{-3}, a salty southern in-

TABLE 1. Latitudinal range, maximum neutral density, and maximum pressure of the quasi-zonal tropical currents at 165°E and 125°W (see Fig. 4).

	Latitude range		Max. γ_n (kg m^{-3})		Max pressure (dbar)	
Current	165°E	125°W	165°E	125°W	165°E	125°W
STCC	18°–20°N	—	26.2	—	350	—
NEC[a]	11°–20°N	12°–18°N	27.3/26.2	27.3	700/350	700
	9°–11°N	—	26.9	—	400	—
NECC	2°–8°N	6°–11°N	26.7	26.7	300	250
NSCC[b]	2°–4°N	3°–6°N	27.2/26.5	27.0/26.3	600/250	500/160
EUC[b]	2°S–2°N	2°S–2°N	26.7/25.5	26.5/26.0	350/200	250/150
SSCC[b]	4°–2°S	6°–3°S	27.2/26.5	27.0/26.3	600/250	500/160
SEC[c]	3°S–1°N	3°S–4°N	25.5	25.0	250	100
	20°–3°S	20°–5°S	27.3–26.5	27.3–26.2	700–280	700–150
SECC	11°–5°S	—	25.5	—	220	—

[a] The second γ_n and pressure are the NEC upper limits under the STCC from 18° to 20°N.
[b] The second γ_n and pressures are the subsurface cores of these currents.
[c] The maximum γ_n and pressures of the SEC vary with latitude over the noted ranges.

fluence is present within the entire deep equatorial pycnostad, now between 5°S and 5°N. Again local meridional extrema are advected eastward at the poleward edges of the SCCs, now 6° from the equator. Around this same density, a homogenous local vertical maximum between 7°N and 13°N is the result of mixing within the center of the northern deep cyclonic gyre. All these deep equatorial influences are poleward of and shallower than their locations at 165°E, consistent with potential vorticity conservation below eastward pycnocline shoaling. In addition, these influences are about 0.3 kg m^{-3} lighter at 125°W than at 165°E, suggestive of diapycnal mixing.

At 165°E, the pycnocline is strongest at $\gamma_n = 23.5$ kg m^{-3}, and potential vorticity there (Fig. 5a) is of roughly equal magnitude in both hemispheres. STMW is evident at 20°N as a weak minimum at $\gamma_n = 25.5$ kg m^{-3} around the base of the STCC. In the south, there is no corresponding vertical minimum, as 165°E is far from the Southern Hemisphere eastern STMW source. Around $\gamma_n = 26.7$ kg m^{-3}, the equatorial pycnostad is manifest as a subtle local vertical minimum from about 3°S to 3°N (not visible in Fig. 5a). Slightly denser, around $\gamma_n = 27.0$ kg m^{-3}, vertical minima expand poleward to 5°S (barely visible) and 11°N, marking the equatorial influence in the deep cyclonic gyres poleward of the SCCs. As in the property maps (Fig. 3), the southern deep cyclonic gyre is more subtle than the northern deep cyclonic gyre. Within these deep gyres below the pycnocline, the orthogonality of nearly vertical isovorts and nearly horizontal isopycnals suggest an absence of significant adiabatic meridional flows.

At 125°W, potential vorticity (Fig. 5b) is highest in magnitude within the pycnocline, around $\gamma_n = 24.0$ kg m^{-3}, slightly denser but shallower than at 165°E, probably because the mixed layer is lighter and deeper in the west. Potential vorticity is high under the ITCZ from 9°N to 13°N, where the pycnocline is closest to the surface. This maximum, much higher than at 165°E, precludes direct meridional flow. As shown above (Fig. 3), water within the pycnocline must circumnavigate the high potential vorticity under the ITCZ on its way from the subtropics to the equator. At 20°N, the local vertical minimum at $\gamma_n = 24.5$ kg m^{-3} is a signature of eastern STMW that underlies the NPTW salinity maximum. In the Southern Hemisphere eastern STMW is much more clearly evident as a broad vertical minimum between $\gamma_n = 25.0$ kg m^{-3} and $\gamma_n = 26.0$ kg m^{-3}. The meridional homogeneity in Southern Hemisphere eastern STMW is the result of stratification increasing linearly toward the equator to compensate the shrinking Coriolis parameter and conserve potential vorticity. Hence in contrast to the northern pycnocline, there is no impediment to direct meridional flow toward the equator within the southern pycnocline. Around $\gamma_n = 26.5$ kg m^{-3}, the deep equatorial pycnostad is evident in the local vertical minimum from 5°S to 5°N. Slightly denser, around $\gamma_n = 26.8$ kg m^{-3}, vertical minima expand poleward to 10°S (barely visible) and 13°N, marking the equatorial influence in the deep cyclonic gyres poleward of the SCCs. As in the salinity field, these deep equatorial influences are all poleward of, lighter than, and shallower than analogous features at 165°E. The poleward spread of low potential vorticity below the pycnocline from west to east suggests deep interior meridional flow is poleward in the presence of eastward zonal flow.

In summary, these two sections show the shoaling and strengthening of the pycnocline from west to east. Poleward shifts of the NEC and NECC from west to east are apparent, as are shoalings and poleward shifts of the SCCs. The salinity sections show the contrast at the equator between the strong salty SPTW in the southeast and the combined fresh northern influence of CCW in the northeast, surface water under the ITCZ, and NPIW in the northwest. Lateral extrema within the SCCs and the eastern EUC are suggestive of eastward zonal advection. The deeper homogeneity in salinity between the deep SEC and the SSCC, as well as between the deep NEC and the NSCC, suggests mixing within deep cyclonic gyres bounded by these currents. These

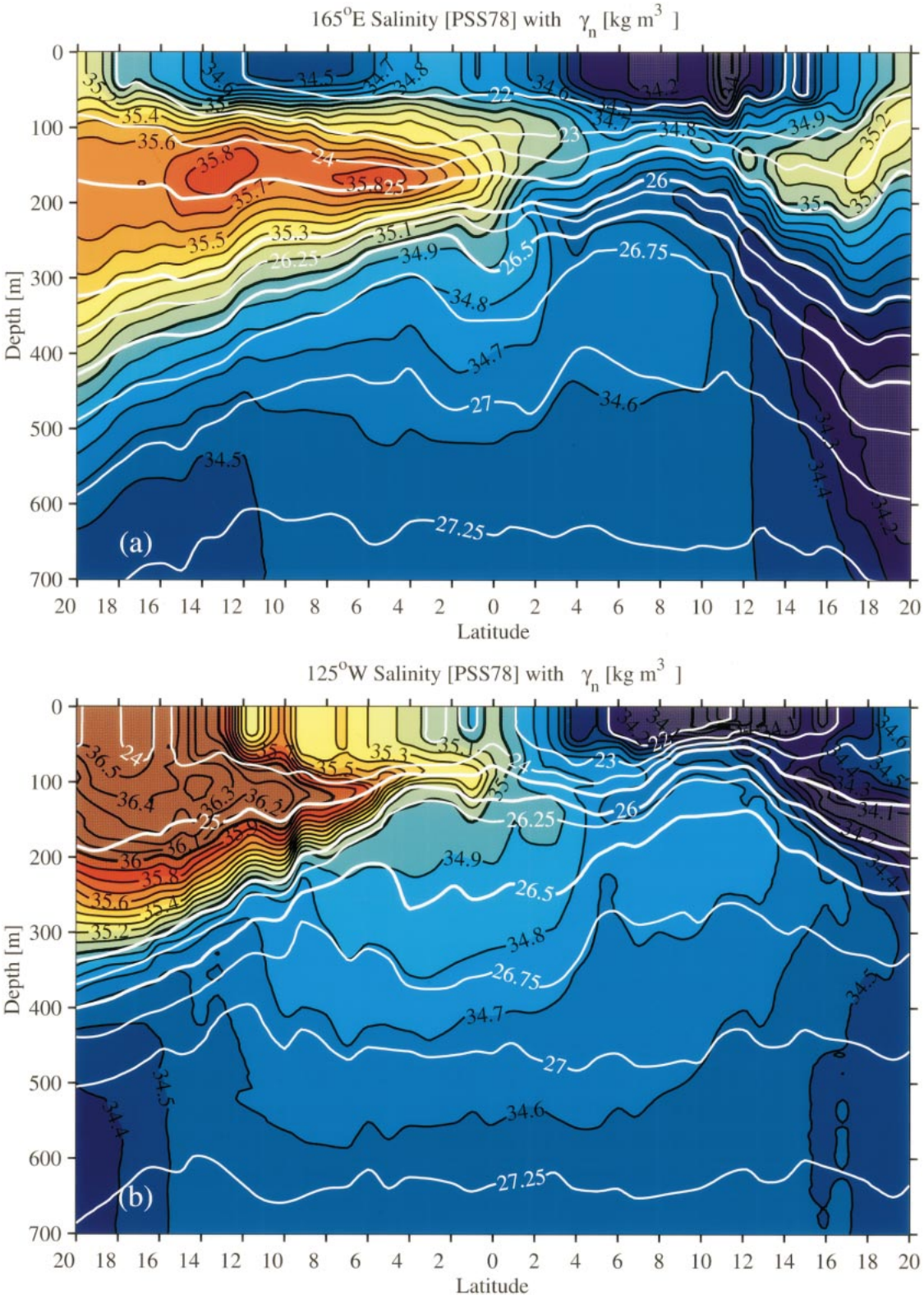

FIG. 4. Mean meridional–vertical sections of salinity contoured at 0.1 intervals (PSS-78) with contours of γ_n at varying intervals (thick lines 25.0, 26.0, and 26.5 kg m^{-3}) overlaid in white. Color palettes follow Fig. 2. Nominal vertical exaggeration is 5000: 1. (a) 165°E. (b) 125°W.

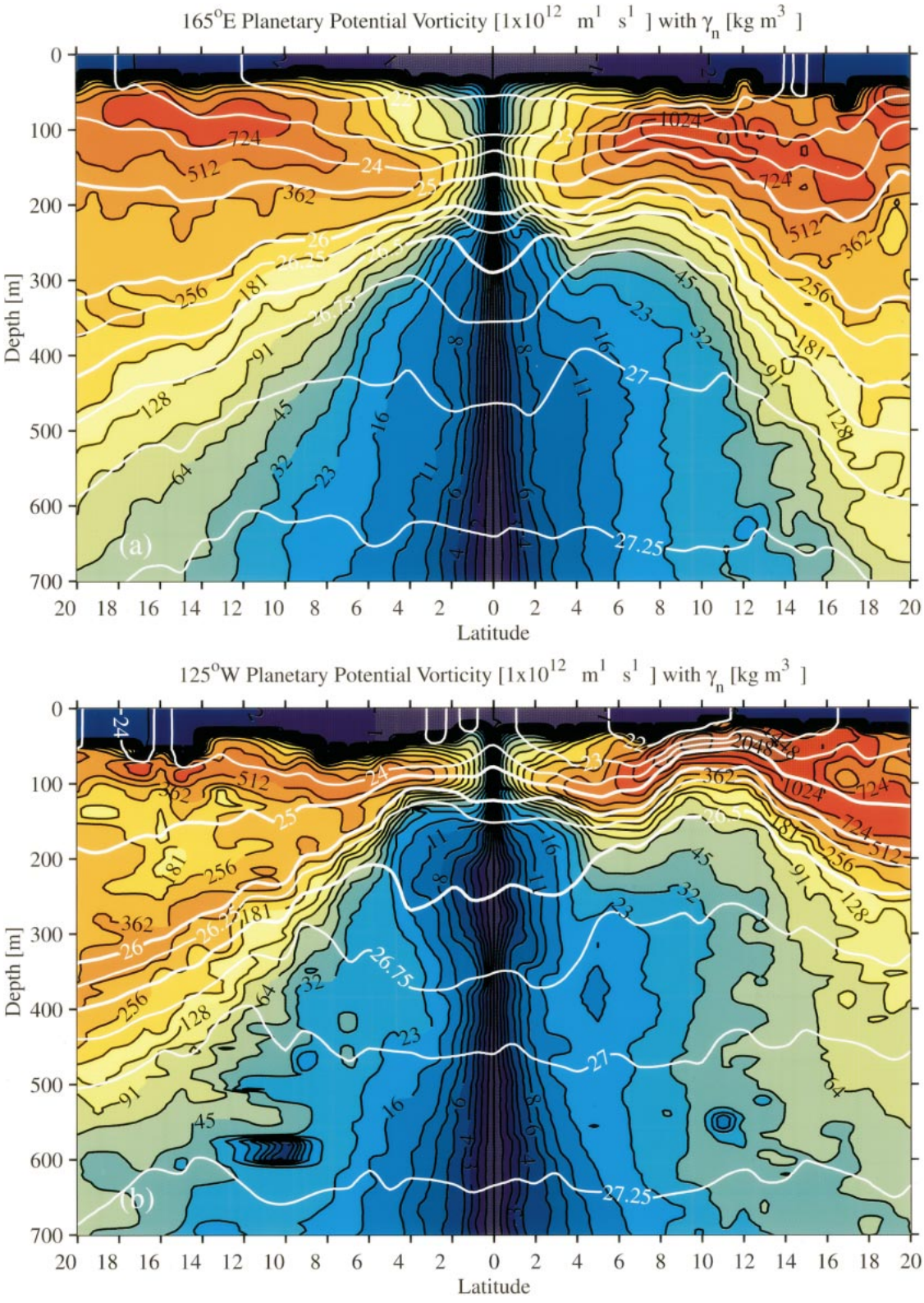

FIG. 5. Mean meridional–vertical sections of planetary potential vorticity contoured at logarithmic intervals (10^{-12} m^{-1} s^{-1}) with contours of γ_n at varying intervals (thick lines 25.0, 26.0, and 26.5 kg m^{-3}) overlaid in white. Color palettes follow Fig. 2. Nominal vertical exaggeration is 5000:1. (a) 165°E. (b) 125°W.

gyres are associated with a lack of interior meridional convergence toward the equator across the Pacific in both hemispheres. The potential vorticity sections highlight the contrast between the Southern and Northern Hemisphere pycnoclines, with the ridge of high potential vorticity under the ITCZ presenting an obstacle to direct meridional flow in the northeast, but smaller barriers in the west, and no such impediment in the southeast. STMWs are evident as vertical minima in potential vorticity under salinity maxima in the northwest and especially in the southeast. In addition, the low potential vorticity and high salinity within the deep cyclonic gyres in each hemisphere is consistent with a lack of equatorward convergence below the pycnocline. In fact, poleward spreading of these equatorial influences to the east between the SSCC and the deep SEC and between the deep NEC and the NSCC supports arguments for a deep poleward interior flow.

5. Interior quasi-meridional geostrophic mass transport estimates

Geostrophic calculations are made relative to a reference surface of 900 dbar, roughly $\gamma_n = 27.5$ kg m^{-3}. Inspection of the depth of this isopycnal (not shown) suggests that geostrophic shear at this surface is weak except in the far southwest portion of the region under investigation, where the subtropical pycnocline is deep. This assumption is supported by direct measurements at this level (Davis 1998). The 900-dbar surface sits well beneath the tropical pycnocline and its use as a reference surface captures all the geostrophic shear above. Three previous quantitative works on zonal mass transports across the Tropics used similar surfaces: 600 dbar at 165°E (Gouriou and Toole 1993), 1000 dbar between 150° and 158°W (Wyrtki and Kilonsky 1984), and 500 dbar at 110°W (Hayes et al. 1983).

Quasi-meridional interior geostrophic mass transport estimates presented here are made in a layer extending from the base of the mixed layer to the base of the tropical pycnocline. The results are similar to those inferred independently from wind fields using Sverdrup dynamics (McPhaden and Fine 1988), but here the magnitudes of the interior meridional transports are quantified as well as the density range over which they occur. The mixed layer is excluded because the mean wind field over nearly the entire region dictates a poleward Ekman transport (Lu and McCreary 1995), which overwhelms the equatorward geostrophic velocity in the mixed layer. Our functional definition of the tropical pycnocline base in this instance is the neutral density at which the net interior meridional mass transport changes sign from equatorward above to poleward below within a 9° latitude band containing the deep cyclonic gyres in each hemisphere. In the Northern Hemisphere, from 3° to 11°N, the base sits at $\gamma_n = 25.9 \pm 0.2$ kg m^{-3}. In the Southern Hemisphere, from 4° to 12°S, the base sits at $\gamma_n = 26.2 \pm 0.2$ kg m^{-3} (see Fig. 1 for isopycnal winter outcrop locations). Interior meridional transports at 8°N and 8°S show convergent equatorward flow, hence interior communication from the subtropics to the equator above these isopycnals and divergent poleward flow in the deep cyclonic gyres below them (Fig. 6). Only interior transports are presented here. While western boundary currents in both hemispheres transport significant amounts of subtropical pycnocline water toward the equator, they have been extensively discussed elsewhere (Tsuchiya et al. 1989; Lukas et al. 1991; Butt and Lindstrom 1994; Wijffels et al. 1995).

In the Southern Hemisphere, meridional mass transport estimates within the pycnocline, from $\gamma_n = 26.2$ kg m^{-3} to the base of the mixed layer, are made from 17°S equatorward. South of 17°S data starts too far off the South American coast for a meaningful interior meridional transport estimate. At all latitudes the interior meridional transport ends well east of the western boundary, and equatorward of 14°S this transport starts west of South America. The interior transport occurs between 135°W and South America at 17°S, but shifts westward toward the equator and is found between 170°W and 110°W by 6°S. Between 17°S and 6°S the estimates have a minimum of $13(\pm 5) \times 10^9$ kg s^{-1} at 9°S and a maximum of $19(\pm 2) \times 10^9$ kg s^{-1} at 16°S, both latitudes where data are sparse and error estimates are large. From 17°S to 6°S the weighted average and standard deviation of interior meridional mass transport is $15(\pm 1) \times 10^9$ kg s^{-1} (Fig. 7a). This value is an estimate of the interior subtropical mass transport from the Southern Hemisphere toward the equator. For purposes of comparison, this interior meridional mass transport estimate slightly exceeds the 9–12 ($\times 10^6$ m^3 s^{-1}) of southern origin estimated to join the EUC core from western boundary currents in the Southern Hemisphere (Butt and Lindstrom 1994). These results are in reasonable accord with analysis of a data assimilation product which suggest western boundary and interior transports at 10°S of 15 and 11 ($\times 10^6$ m^3 s^{-1}), respectively (Huang and Liu 1998).

Equatorward of 6°S, meridional interior transport estimates increase from $20(\pm 2) \times 10^9$ kg s^{-1} between 170°W and 110°W at 5°S to $30(\pm 4) \times 10^9$ kg s^{-1} between 170°W and 120°W at 3°S. While low-latitude geostrophic calculations are noisy, the trend is clear. This rapid increase probably reflects the presence of a shallow meridional overturning cell at the equator, with interior equatorward geostrophic transport working to offset large poleward mass transports in the Ekman layer. This cell has been observed in profiling and acoustic Doppler current meter data from the Hawaii–Tahiti Shuttle Experiment (McPhaden 1984; Johnson and Luther 1994) and reproduced in numerical models (Lu et al. 1998).

The Northern Hemisphere is somewhat more complicated than the Southern Hemisphere, with the quasi-zonal NEC, NECC, SEC, and EUC alternating in flow

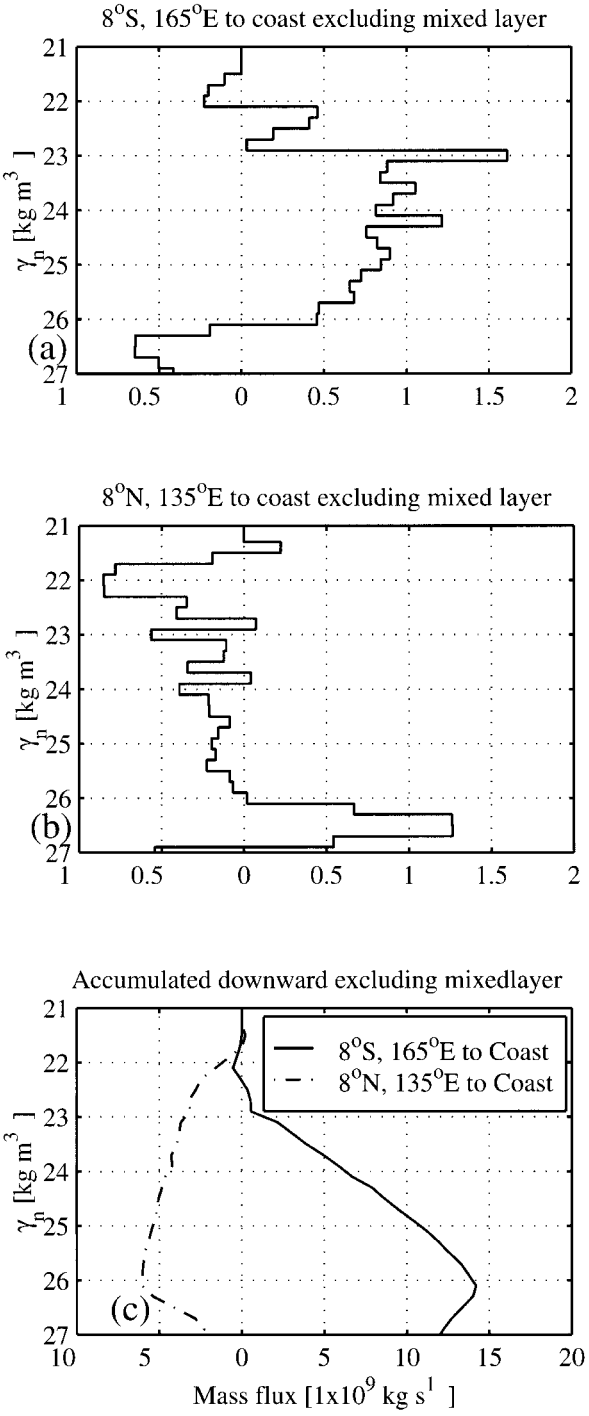

FIG. 6. Net meridional mass transport (10^9 kg s^{-1}) excluding the mixed layer binned in γ_n every 0.2 kg m^{-3} from the South American coast to (a) 165°E at 8°S and (b) 135°E at 8°N. In the south, equatorward flow is concentrated near the eastern STMW density and poleward flow below γ_n = 26.1 kg m^{-3}. In the north, equatorward flow is at lighter densities and poleward flow below γ_n = 25.9 kg m^{-3}. (c) Downward accumulated integrals of (a) and (b) show the net interior transport within the pycnocline (to γ_n roughly 26 kg m^{-3}) in the Northern Hemisphere (6×10^9 kg s^{-1}) is much less than that in the Southern Hemisphere (14×10^9 kg s^{-1}).

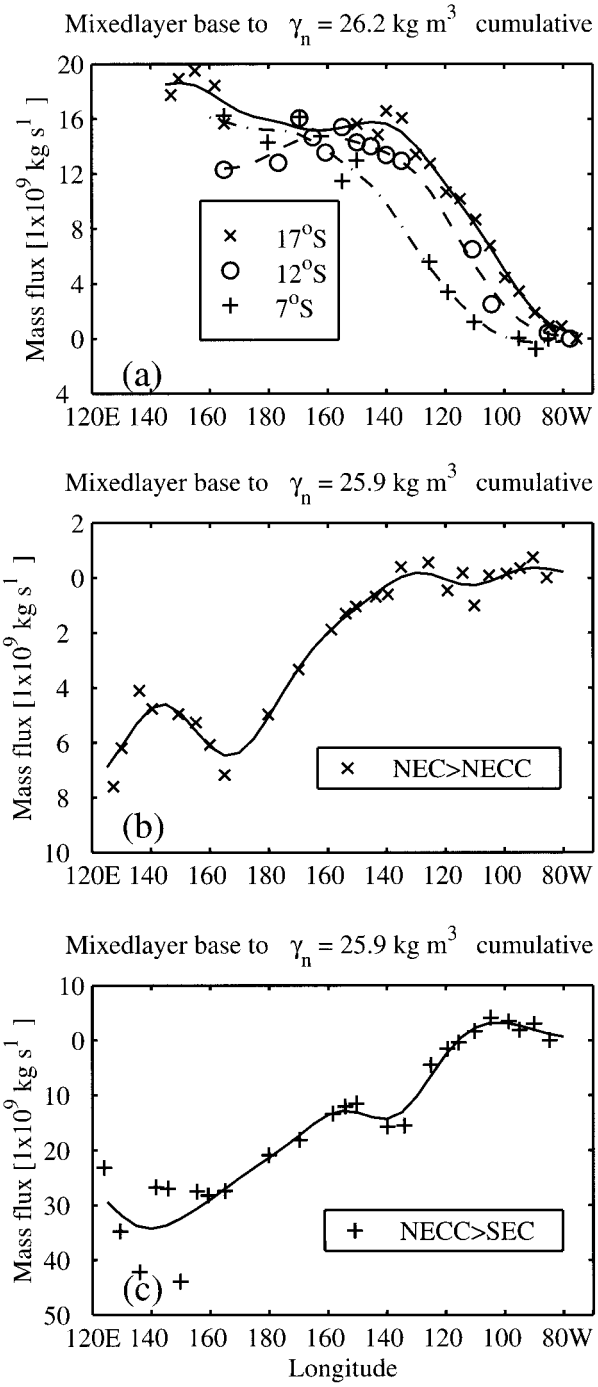

FIG. 7. Quasi-meridional interior pycnocline (mixed layer base to pycnocline base) mass transport (10^9 kg s^{-1}) zonally accumulated from the Americas westward. Symbols are individual integration points and lines are objectively mapped assuming a Gaussian covariance with a correlation length scale of 20° longitude and an error-to-signal energy of 0.25. (a) Southern Hemisphere transports at three latitudes (17°S solid line, 12°S dashed, and 7°S dot–dashed) with a pycnocline base at γ_n = 26.2 kg m^{-3}. (b) Northern Hemisphere transport between the NEC and NECC with a pycnocline base at γ_n = 25.9 kg m^{-3}. (c) Northern Hemisphere transport between the NECC and SEC with a pycnocline base at γ_n = 25.9 kg m^{-3}.

direction. Instead of presenting simple meridional mass transports, which would contain portions of these quasi-zonal currents, we isolate the cross-gyre transports by calculating transports across the geopotential anomaly trough under the ITCZ that separates the NEC from the NECC (Fig. 7b). Another estimate is made across the lower-latitude ridge that separates the NECC from the SEC and 2°N at a few western longitudes where no ridge is evident (Fig. 7c). In both cases, there are regions of little net transport east and west of where the interior meridional transport occurs. Within the pycnocline, from $\gamma_n = 25.9$ kg m^{-3} to the base of the mixed layer, $-5(\pm 1) \times 10^9$ kg s^{-1} flows across the trough from the NEC to the NECC between 165°E and 135°W. This value is an estimate of the interior subtropical mass transport from the Northern Hemisphere toward the equator, and is one third the estimate of $15(\pm 1) \times 10^9$ kg s^{-1} equatorward interior flow estimated for the Southern Hemisphere. A simple comparison of interior pycnocline meridional mass transports along 8°N and 8°S gives a similar result (Fig. 6c). The Northern Hemisphere interior transport estimate is probably an upper bound because it may contain southward flow from a tropical recirculation around the ITCZ centered near 11°N, 125°W (Fig. 2b). However, since there is no evidence of any significant northward component of the recirculation east of 125°W (Fig. 7b), the net tropical recirculation is likely to be small. For purposes of comparison, this northern interior transport is less than half of the 13–16 ($\times 10^6$ m^3 s^{-1}) of northern origin water estimated to reside within the core of the EUC well to the west at 153°E (Butt and Lindstrom 1994). These results are again in reasonable accord with analysis of a data assimilation product, which suggests western boundary and interior transports at 10°N of 14 and 3×10^6 m^3 s^{-1}, respectively (Huang and Liu 1998).

Farther to the south, an estimated $-35(\pm 8) \times 10^9$ kg s^{-1} flows across the low-latitude ridge from the NECC to the SEC between 165°E and 105°W (Fig. 7c). The $30(\pm 8) \times 10^9$ kg s^{-1} increase in equatorward transport with relation to the northern estimate seems large and may be an upper bound, since part of the transport calculation is made at 2°N, a fairly low latitude at which to apply geostrophy. However, this increase can fairly easily be accounted for by a combination of two similarly sized sources. First, the addition of northern subtropical water from the Mindanao Current (Lukas et al. 1991; Wijffels et al. 1995) at the western boundary transported eastward within the NECC could be contributing to equatorward pycnocline mass flux. The NECC carries 20×10^6 m^3 s^{-1} at 165°E (Gouriou and Toole 1993) and only 8×10^6 m^3 s^{-1} by 110°W (Hayes et al. 1983), allowing for an increase of 12×10^6 m^3 s^{-1} in equatorward transport from the NECC to the SEC. Second, the poleward Ekman transport across the low-latitude ridge is 45×10^9 kg s^{-1} between 165°E and 105°W using the Hellerman and Rosenstein (1983) surface wind stress climatology after applying a recommended scaling factor of 0.8 to correct the drag coefficient (Harrison 1989). If 40 (±25)% of the equatorward geostrophic transport balancing this Ekman transport occurs in a shallow tropical meridional cell extending below the mixed layer (Lu et al. 1998), it would account for the remaining mass budget within interior meridional transport errors.

6. Discussion

The focus of this manuscript is on describing interior pycnocline pathways from the subtropics to the equator in the Pacific Ocean and quantifying mass fluxes of these pathways. The serpentine pathway in the Northern Hemisphere has been described using the potential vorticity and salinity fields, as well as quantified with geostrophic calculations. Relatively fresh water flows westward in the NEC, skirting the high potential vorticity under the ITCZ, then flows south from the NEC to the NECC between 165°E and 135°W, then eastward in the NECC, then south between 150°W and 100°W to join the SEC and flow westward and converge on the EUC. The more direct interior pathway in the Southern Hemisphere has also been studied, with salty low potential vorticity water flowing northward and westward. At 17°S this flow occurs between 135°W and the South American coast and by 6°S between 170°W and 110°W, continuing northward and westward to the equator, augmented by a shallow meridional overturning cell.

The Southern Hemisphere interior route carries about three times more subtropical water towards the equator than does the northern interior route. At least two, probably related, factors contribute to this difference. First, a large body of modeling work reviewed in the introduction as well as the data analysis presented here has demonstrated that high potential vorticity under the ITCZ is obviously linked to the relatively small equatorward interior flow found in the north. Most equatorward flow in the Northern Hemisphere pycnocline flows around this region of high potential vorticity to the western boundary where it can more easily turn southward. Second, there is evidence for a hemispheric asymmetry in eastern STMW production rates and locations. The Northern Hemisphere region of high subduction rate associated with eastern STMW production is centered near 25°N, 130°W (Huang and Qiu 1994; Hautala and Roemmich 1998). The analogous southern region is centered near 20°S, 120°W (Huang and Qiu 1998). The area of large subduction rate associated with eastern STMW production in the south is nearly twice the magnitude and twice the area of that in the north. In addition the southern region is located eastward and equatorward of the northern region. All of these differences contribute to a stronger equatorward interior flux of eastern STMW in the Southern Hemisphere. The low potential vorticity evident in the pycnocline of the Southeast Pacific (Figs. 2d and 5b) as well as the large equatorward transport of water around the density of eastern STMW

in the south compared to that in the north (Fig. 6) reflect this asymmetry in production rates and locations.

The other significant result of this manuscript is that the salinity, potential vorticity, and geostrophic velocity fields are all consistent with deep cyclonic gyres below the pycnocline, hence an absence of interior equatorward flow of subtropical water there. The poleward interior flows of these gyres are in opposition to the equatorward flows within the pycnocline, the base of which we defined to be near the 26 kg m^{-3} neutral surface. The eastward flowing SCCs serve as the equatorward limbs of these deep cyclonic gyres and the deeper portions of the westward flowing NEC and SEC serve as their poleward limbs. Salinity and potential vorticity signals are advected around these gyres, with reduced meridional gradients in the gyre interiors.

The dynamics of these deep gyres are not clear. In addition to the cyclonic gyres poleward of the SCCs there is evidence for anticyclonic gyres equatorward of the SCCs (Rowe et al. 2000). The eastward zonal flows within the SCCs have been modeled as inertial jets (Johnson and Moore 1997). The westward quasi-zonal return flows poleward of the SCCs are part of the deep NEC and SEC, but are not well studied. More return flow equatorward of the SCCs may be in the Equatorial Intermediate Current (Rowe et al. 2000). Flows completing the gyres at the western boundaries presumably follow western boundary current dynamics. Examination of acceleration potential and potential vorticity (Figs. 3b and 3d) suggests that in both deep cyclonic gyres contours of these quantities cross in the western boundary, where dissipation is expected. Upwelling under the ITCZ and off the South American coast may force the poleward flow within these deep cyclonic gyres through vortex stretching and diapycnal processes. In the southern deep gyre the effects of upwelling are likely confined to the coast, and are not well resolved with this dataset. However, in the northern deep gyre contours cross again in the region of poleward flow under the ITCZ, where vortex stretching and diapycnal processes are posited. The eastward lightening of the equatorial influences in these deep gyres discussed here, as well as the change in density of the SCCs (Johnson and Moore 1997) is consistent with the hypothesized influence of diapycnal processes.

Acknowledgments. This work was stimulated by conversations with E. Firing, W. Kessler, J. McCreary, D. Rowe, and, as always, L. Thompson. E. Firing, W. Kessler, J. McCreary, and an anonymous review all helped to improve the manuscript. K. McTaggart helped with calibration and processing of CTD data. This work was funded by the NOAA Office of Oceanic and Atmospheric Research, the NOAA Office of Global Programs, and the NASA Physical Oceanography Program.

REFERENCES

Akima, H., 1970: A new method of interpolation and smooth curve fitting based on local procedures. *J. Assoc. Comput. Mach.,* **17,** 589–603.

Butt, J., and E. Lindstrom, 1994: Currents of the east coast of New Ireland, Papua New Guinea, and their relevance to the regional undercurrents in the Western Equatorial Pacific Ocean. *J. Geophys. Res.,* **99,** 12 503–12 514.

Davis, R. E., 1998: Preliminary results from directly measuring middepth circulation in the tropical and South Pacific. *J. Geophys. Res.,* **103,** 24 619–24 639.

Deser, C., M. A. Alexander, and M. S. Timlin, 1996: Upper-ocean thermal variations in the North Pacific during 1970–1991. *J. Climate,* **9,** 1840–1855.

Fine, R. A., W. H. Peterson, and H. G. Ostlund, 1987: The penetration of tritium into the tropical Pacific. *J. Phys. Oceanogr.,* **17,** 553–564.

Gouriou, Y., and J. Toole, 1993: Mean circulation of the upper layers of the western equatorial Pacific Ocean. *J. Geophys. Res.,* **98,** 22 495–22 520.

Gu, D., and G. S. Philander, 1997: Interdecadal climate fluctuations that depend on exchanges between the tropics and extratropics. *Science,* **275,** 805–807.

Harrison, D. E., 1989: On climatological monthly mean wind stress and wind stress curl fields over the World Ocean. *J. Climate,* **2,** 57–70.

Hautala, S. L., and D. H. Roemmich, 1998: Subtropical mode water in the Northeast Pacific Basin. *J. Geophys. Res.,* **103,** 13 055–13 066.

Hayes, S. P., J. M. Toole, and L. J. Mangum, 1983: Water-mass and transport variability at 110°W in the Equatorial Pacific. *J. Phys. Oceanogr.,* **13,** 153–168.

Hellerman, S., and M. Rosenstein, 1983: Normal monthly wind stress over the world ocean with error estimates. *J. Phys. Oceanogr.,* **13,** 1093–1104.

Hoffman, E. E., A. J. Busalacchi, and J. J. O'Brien, 1981: Wind generation of the Costa Rica Dome. *Science,* **214,** 552–554.

Huang, B., and Z. Liu, 1999: Pacific subtropical–tropical thermocline water exchange in the National Centers for Environmental Prediction ocean model. *J. Geophys. Res.,* **104,** 11 065–11 076.

Huang, R. X., and B. Qiu, 1994: Three-dimensional structure of the wind-driven circulation in the subtropical North Pacific. *J. Phys. Oceanogr.,* **24,** 1608–1622.

——, and ——, 1998: The structure of the wind-driven circulation in the subtropical South Pacific Ocean. *J. Phys. Oceanogr.,* **28,** 1173–1186.

Jackett, D., and T. J. McDougall, 1997: A neutral density variable for the world's ocean. *J. Phys. Oceanogr.,* **27,** 237–263.

Johnson, E. S., and D. S. Luther, 1994: Mean zonal momentum balance in the upper and central equatorial Pacific Ocean. *J. Geophys. Res.,* **99,** 7689–7705.

Johnson, G. C., and D. W. Moore, 1997: The Pacific subsurface countercurrents and an inertial model. *J. Phys. Oceanogr.,* **27,** 2448–2459.

Levitus, S., and T. P. Boyer, 1994: *World Ocean Atlas 1994.* Vol. 4: *Temperature: NOAA Atlas NESDIS 4,* U.S. Govt. Printing Office, 117 pp.

——, R. Burgett, and T. P. Boyer, 1994: *World Ocean Atlas 1994.* Vol. 4: *Salinity: NOAA Atlas NESDIS 3,* U.S. Govt. Printing Office, 99 pp.

Liu, Z., 1994: A simple model of the mass exchange between the subtropical and tropical ocean. *J. Phys. Oceanogr.,* **24,** 1153–1165.

——, and B. Huang, 1998: Why is there a tritium maximum in the central equatorial Pacific thermocline? *J. Phys. Oceanogr.,* **28,** 1527–1533.

——, S. G. H. Philander, and R. C. Pacanowski, 1994: A GCM study of the tropical-subtropical upper-ocean water exchange. *J. Phys. Oceanogr.,* **24,** 2606–2623.

Lu, P., and J. P. McCreary Jr., 1995: Influence of the ITCZ on the flow of thermocline water from the subtropical to the equatorial Pacific Ocean. *J. Phys. Oceanogr.,* **25,** 3076–3088.

——, ——, and B. A. Klinger, 1998: Meridional circulation cells and the source waters of the Pacific equatorial undercurrent. *J. Phys. Oceanogr.,* **28,** 62–84.

Lukas, R., E. Firing, P. Hacker, P. L. Richardson, C. A. Collins, R. Fine, and R. Gammon, 1991: Observations of the Mindanao Current during the Western Equatorial Pacific Ocean Circulation Study. *J. Geophys. Res.,* **96,** 7089–7104.

Luyten, J. R., J. Pedlosky, and H. Stommel, 1983: The ventilated thermocline. *J. Phys. Oceanogr.,* **13,** 292–309.

Lysne, J., P. Chang, and B. Giese, 1997: Impact of the extratropical Pacific on equatorial variability. *Geophys. Res. Lett.,* **24,** 2589–2592.

McCreary, J. P., and P. Lu, 1994: On the interaction between the subtropical and the equatorial oceans: The subtropical cell. *J. Phys. Oceanogr.,* **24,** 466–497.

McPhaden, M. J., 1984: On the dynamics of the equatorial subsurface countercurrents. *J. Phys. Oceanogr.,* **14,** 1216–1225.

——, and R. A. Fine, 1988: A dynamical interpretation of the tritium maximum in the Central Equatorial Pacific. *J. Phys. Oceanogr.,* **18,** 1454–1457.

Rothstein, L. M., R.-H. Zhang, A. J. Busalacchi, and D. Chen, 1998: A numerical simulation of the mean water pathways in the subtropical and tropical Pacific Ocean. *J. Phys. Oceanogr.,* **28,** 322–342.

Rowe, G. D., E. Firing, and G. C. Johnson, 2000: Pacific equatorial subsurface contour currents' velocity, transport, and potential vorticity. *J. Phys. Oceanogr.,* in press.

Schneider, N., A. J. Miller, M. A. Alexander, and C. Deser, 1999: Subduction of decadal North Pacific temperature anomalies: Observations and dynamics. *J. Phys. Oceanogr.,* **29,** 1056–1070.

Tsuchiya, M., 1968: Upper waters of the intertropical Pacific Ocean. *Johns Hopkins Oceanogr. Stud.,* No. 4, 50 pp.

——, 1975: Subsurface countercurrents in the eastern equatorial Pacific Ocean. *J. Mar. Res.,* **33** (Suppl.), 145–175.

——, R. Lukas, R. A. Fine, E. Firing, and E. Lindstrom, 1989: Source waters of the Pacific Equatorial Undercurrent. *Progress in Oceanography,* Vol. 23, Pergamon, 101–147.

Wijffels, S., E. Firing, and J. Toole, 1995: The mean structure and variability of the Mindanao Current at 8°N. *J. Geophys. Res.,* **100,** 18 421–18 435.

Wyrtki, K., 1975: Fluctuations of dynamic topography in the Pacific Ocean. *J. Phys. Oceanogr.,* **5,** 450–459.

——, and B. Kilonsky, 1984: Mean water and current structure during the Hawaii-to-Tahiti shuttle experiment. *J. Phys. Oceanogr.,* **14,** 242–254.

Zhang, R.-H., L. M. Rothstein, and A. J. Busalacchi, 1998: Origin of upper-ocean warming and El Niño change on decadal scales in the tropical Pacific Ocean. *Nature,* **391,** 879–883.